ACS Catalysis

Research Article

Cite This: ACS Catal. 2019, 9, 8996−9008

pubs.acs.org/acscatalysis

Microkinetic Model of Propylene Oligomerization on Brønsted Acidic Zeolites at Low Conversion

Sergio Vernuccio,[†] Elizabeth E. Bickel,[‡] Rajamani Gounder,[‡] and Linda J. Broadbelt*[,†]

[†]Department of Chemical and Biological Engineering, Northwestern University, Evanston, Illinois 60208, United States

[‡]Davidson School of Chemical Engineering, Purdue University, West Lafayette, Indiana 47907, United States

Supporting Information

ABSTRACT: The construction of a computational framework that describes the kinetic details of the propylene oligomerization reaction network on Brønsted acidic zeolites is particularly challenging due to the considerable number of species and reaction steps involved in the mechanism. This work presents a detailed microkinetic model at the level of elementary steps that includes 4243 reactions and 909 ionic and molecular species within the C_2−C_9 carbon number range. An automated generation procedure using a set of eight reaction families was applied to construct the reaction network. The kinetic parameters for each elementary step were estimated using transition state theory, Evans−Polanyi relationships, and thermodynamic data. The reaction mechanism and its governing kinetic parameters were embedded into the design equation of a plug-flow reactor, which was the reactor configuration used to experimentally measure reactant and product concentrations as a function of propylene conversion and temperature on a representative H-ZSM-5 (MFI) zeolite. The resulting mechanistic model is able to accurately describe the experimental data over a wide range of operating conditions in the low propylene conversion (<4%) regime. The agreement between experimentally measured propylene conversion and product selectivities and the model results demonstrates the robustness of the model and the approach used to develop it to simulate the kinetic behavior of this complex reaction network.

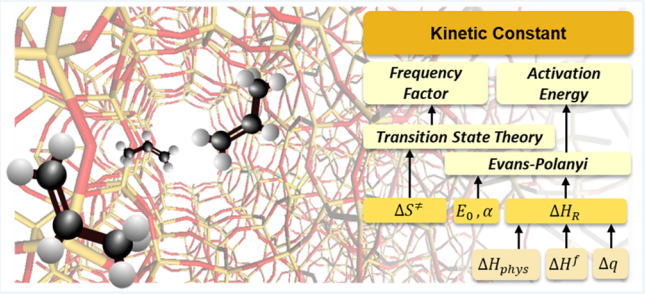

KEYWORDS: *oligomerization, propylene, kinetic model, zeolite, H-ZSM-5*

1. INTRODUCTION

The direct conversion of light olefins into heavier oligomers over Brønsted acid catalysts is an economically attractive strategy to upgrade shale gas feedstocks into liquid products. The increased availability of shale resources and their consequent decreased cost over the past decade have attracted significant interest in their conversion into chemicals and liquid transportation fuels.[1−4] A typical process for the conversion of light olefins to gasoline range products ($<C_{12}$) is based on the use of shape-selective Brønsted acidic zeolites such as H-ZSM-5 (MFI),[5,6] because Brønsted acid sites that charge-compensate framework Al atoms in zeolites are reactive toward unsaturated olefinic molecules. The application of this family of zeolites was originally proposed as a potential replacement for solid phosphoric acid catalysts, in the olefins-to-gasoline process developed by Mobil to convert light olefins from fluid catalytic cracking (FCC).[7−11]

The olefin oligomerization reaction sequence over acidic zeolites can be rationalized in terms of alkylation chemistry, where the first step is the protonation of a physisorbed olefin by a Brønsted acid site to form an ionic intermediate, followed by addition of an olefin to form a higher carbon number intermediate, and finally deprotonation to form a heavier product olefin. This process is highly exothermic and results in a net decrease in the number of molecules[12] upon the formation of true oligomers, which are the products expected from dimerization and subsequent oligomerization reactions of the olefin monomer reactant.[13] These oligomers can further undergo skeletal isomerization and cracking via β-scission, resulting in a mixture of olefins including carbon numbers that are not integer multiples of the initial monomer. These reactions contribute to modifying the molecular weight distribution of the products, resulting in large and highly interconnected reaction networks.

The typical approach that is applied to study these complex reacting systems is "pathways-level modelling", which consists of lumping of several reactions into a single one describing the conversion of a reagent into a product and disregarding any reaction intermediate(s).[14−16] In lumped kinetic models, several compounds are grouped together based on their molecular properties, such as the carbon number. These models are relatively easy to develop because the number of lumps and the number of reactions considered are limited; however, molecular information is obscured by the multi-component nature of each lump. Furthermore, the use of these models is usually associated with several assumptions, for

Received: May 18, 2019
Revised: August 13, 2019
Published: August 21, 2019

DOI: 10.1021/acscatal.9b02066
ACS Catal. 2019, 9, 8996−9008

Table 1. List of Reaction Families Proposed for the Oligomerization of Propylene on Acidic Zeolites at Low Conversion[a]

Protonation	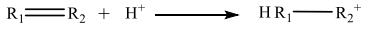
Deprotonation	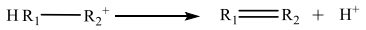
Oligomerization	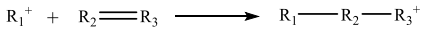
β-Scission	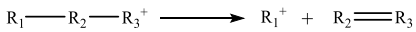
Hydride Shift	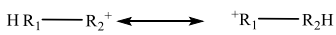
Methyl Shift	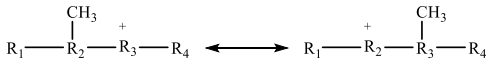
α-PCP-Branching	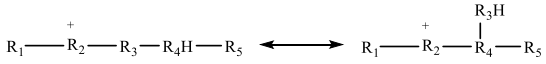
β-PCP-Branching	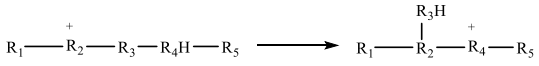

[a]Extracted from ref 17. Copyright 2019 by John Wiley & Sons, Inc., or related companies.

example, concerning the nature of the rate-determining step(s). This affects the predictive power of the model, rendering its application beyond the range of conditions for which it was specifically developed limited. The alternative proposed in this paper is based on the development of a microkinetic model, which is an attractive method to elucidate the complexity of a large and highly interconnected reaction network. Substantial progress has been made in recent decades regarding automated generation of reaction mechanisms applied to many different types of chemistries and disparate processes.[17] In this work, a detailed reaction network was automatically generated to include each elementary reaction occurring at the Brønsted acid sites in the zeolite catalyst. The reaction rate of each step was expressed by an elementary rate law containing specific kinetic coefficients. All of the involved kinetic parameters are specified based on theoretical considerations and are, for this reason, independent of operating conditions and feed.

The resulting model is able to describe with very good accuracy the salient kinetic details of propylene oligomerization measured experimentally on a representative commercial H-ZSM-5 zeolite at low conversion. The dominant reaction pathways that consume propylene and form oligomeric products are revealed based on net rate analysis.

2. AUTOMATED KINETIC NETWORK GENERATION

The first step in building a microkinetic model to describe the oligomerization of propylene was the automated generation of a reaction network. In this work we employed NetGen, a software package developed by Broadbelt et al.[18,19]

The elementary steps proposed to describe the oligomerization mechanism of the generic olefin C_nH_{2n} are listed below:[20]

$$C_nH_{2n}(g) \leftrightarrow C_nH_{2n}(p) \quad (1)$$

$$C_nH_{2n}(p) + H^+ \leftrightarrow C_nH_{2n+1}{}^+(p) \quad (2)$$

$$C_nH_{2n+1}{}^+(p) + C_nH_{2n}(p) \leftrightarrow C_{2n}H_{4n+1}{}^+(p) \quad (3)$$

$$C_{2n}H_{4n+1}{}^+(p) \leftrightarrow i\text{-}C_{2n}H_{4n+1}{}^+(p) \quad (4)$$

$$C_{2n}H_{4n+1}{}^+(p) \leftrightarrow C_{2n}H_{4n}(p) + H^+ \quad (5)$$

$$C_{2n}H_{4n}(p) \leftrightarrow C_{2n}H_{4n}(g) \quad (6)$$

The suffixes (g) and (p) indicate the gas phase and the pores of the zeolite, respectively. After physisorption of the olefin from the gas phase into the pores of the zeolite (step 1), an ionic intermediate is generated through protonation (step 2). The exact nature of the ionic intermediates (carbenium ion or alkoxide) depends on the specific structure of the bound species, temperature, and geometry of the active site.[21] The resulting chemisorbed ionic intermediate can increase its hydrocarbon chain length by undergoing oligomerization with a physisorbed olefin (step 3) or it can isomerize (step 4), where the symbol *i* before the olefin (step 4) indicates a particular isomer. β-Scission is the reverse step of oligomerization, and it forms a smaller olefin and a smaller ionic species from a larger oligomer. The oligomer product deprotonates (step 5) and desorbs (step 6) from the pore of the zeolite into the gas phase.

The chemical reactions that a physisorbed species can undergo, as specified in steps 2−5, were grouped into reaction families and are listed in Table 1 (extracted from ref 17). The ionic intermediates are referred to herein as carbenium ions for convenience, although their nature can reflect more carbenium ion or more alkoxide character. The isomerization steps include hydride shift, methyl shift, and α and β protonated cyclopropane (PCP) branching. This last isomerization step is postulated to proceed via a PCP intermediate with the charge delocalized over the ring.[22] The subcategories α and β depend on the bond to be broken in the three-membered ring intermediate. These ionic intermediates can also undergo

DOI: 10.1021/acscatal.9b02066
ACS Catal. 2019, 9, 8996−9008

hydride transfer steps to form paraffins, but since the experimental data collected in this study at low conversion (<4%) showed the presence of only minor amounts of paraffins (Figure S1, Table S1, <0.2% of the overall product distribution), the list of reactions considered in Table 1 excludes hydride transfer steps. In this regard, paraffins are considered side products during oligomerization and cracking of light olefins on acidic zeolites.[23−25] In some cases, during the mechanism generation processes, the minor amounts of paraffins that are detected experimentally are lumped with the olefins of the same carbon number in order to reduce calculation efforts,[23,26] which was the approach used here.

In principle, the automated generation process is infinite because oligomerization leads to the formation of higher molecular weight ionic species through consecutive additions of monomers, and the reaction family can be subsequently applied to each product. In this study, a carbon- and rank-based termination criterion $c_i - r_j$[27] was applied, where $i = 9$ and $j = 0$ are, respectively, the maximum number of carbon atoms and the highest rank of the species allowed to react. However, as expected, imposing this termination criterion resulted in the generation of several ionic species of rank 0 and carbon number >9 that were not allowed to react further because of their failure to meet the carbon number criterion. This is a direct consequence of the oligomerization process that produces heavier ionic oligomers that are not associated with any increase in rank. In order to avoid the presence of these unwanted intermediates, the reaction network was limited to ionic and molecular species with a carbon number lower or equal to 9.

3. KINETIC PARAMETER DETERMINATION

3.1. Frequency Factors. The kinetic constants for the elementary steps (1−6) were expressed as a function of temperature following an Arrhenius dependence:

$$k_i = A_i \exp\left(-\frac{B_i}{RT}\right) \tag{7}$$

with

$$B_i = \begin{cases} 0 & i = \text{physisorption} \\ |\Delta H_{\text{phys}}| & i = \text{desorption} \\ E_{\text{a},i} & \text{otherwise} \end{cases} \tag{8}$$

where k is the rate coefficient, A is the Arrhenius pre-exponential factor, R is the universal gas constant, T is the temperature, ΔH_{phys} is the physisorption enthalpy, and E_a is the activation energy. The reverse of physisorption is denoted as "desorption" in eq 8.

The pre-exponential factors were estimated using transition state theory, assuming that every elementary step proceeds through the formation of a transition state or activated complex:[28]

$$A = \left(\frac{k_B T}{h}\right) e^{\Delta S^{\ddagger}/R}\, e^{1-\Delta n^{\ddagger}} (c^0)^{\Delta n^{\ddagger}} \tag{9}$$

where k_B is Boltzmann's constant, h is Planck's constant, $\Delta S^{\ddagger}$ is the entropy change between the reactants and the activated complex, $\Delta n^{\ddagger}$ is the change in the number of moles in going from the reactants to the transition state, and c^0 is the standard state concentration (1 M).

The first term in eq 9 ($k_B T/h$) represents the vibrational frequency along the reaction coordinate, and it is followed by an expression derived from the equilibrium constant between the reactants and transition state. The entropy changes for some of the reactions involved in the network were obtained from data tabulated by Nguyen et al.[29] for isobutene on H-ZSM-5 at 300 K. That study reports an entropy loss in going from physisorbed isobutene and chemisorbed *tert*-butyl ion to the transition state. Vice versa, an entropy gain is reported in going from chemisorbed tert-butoxy ion to the transition state. This indicates that, at industrially relevant temperatures ($T >$ 300 K), the formation of tertiary alkoxides is not entropically favored. Furthermore, in this temperature range, the entropic contribution to Gibbs free energies outweighs the enthalpic contribution of covalent bond formation. As a consequence, the formation of tertiary alkoxides is less favorable than the formation of tertiary carbenium ions within the pores of the zeolite.[21,29] Secondary species, on the other hand, were reported to remain stable as alkoxides in a temperature range of 300−600 K. However, at higher temperatures, the formation of a covalent bond in the alkoxide state introduces an entropic penalty that is not compensated for by the enthalpic gain, resulting in formation of a carbenium ion being more favorable.[21] According to this finding, in the present work which covers a temperature range of 483−523 K, secondary intermediates were treated as alkoxides, while tertiary intermediates were treated as carbenium ions. Primary carbenium ions are commonly not considered as candidate intermediates due to their highly unstable nature,[30,31] but they can be stabilized by interaction with the zeolite framework. For this reason, all primary intermediate species were treated as alkoxides in this study.

The entropy change between reactants and transition states was assumed to be the same for each elementary step within a reaction family involving ionic intermediates with the same alkoxide or carbenium ion character as the reactants. The estimates of the order of magnitude of the frequency factors are listed in Table 2, together with the entropy changes used in the calculation. The frequency factor for alkoxide isomerization was estimated assuming that the entropy change between reactants and transition states is zero. The ratio of frequency factors for physisorption and desorption $\frac{A_{\text{phys}}}{A_{\text{des}}}$ was estimated to be $O(10^{-7})$ according to an entropy loss of 116 J mol^{-1} K^{-1} in going from gas-phase isobutene to the physisorbed state.[29]

Table 2. Order of Magnitude of the Frequency Factors Estimated at 503 K According to Transition State Theory[a]

reaction	$\Delta S^{\ddagger}$ [J mol^{-1} K^{-1}]	$\Delta n^{\ddagger}$	$O(A)$	[−]
protonation	−54	−1	10^4	Pa^{-1} s^{-1}
deprotonation (carbenium ion)	−71	0	10^9	s^{-1}
deprotonation (alkoxide)	23	0	10^{14}	s^{-1}
isomerization (alkoxide)	0	0	10^{13}	s^{-1}

[a] $\Delta S^{\ddagger}$ for protonation and deprotonation are reported in ref 29.

A generalization of these entropy values for unimolecular and bimolecular reactions resulted in the application of the frequency factors calculated for protonation and deprotonation to oligomerization and β-scission by analogy. The frequency factors for all the elementary steps that involved carbenium ions as reactants were calculated from the corresponding ones

DOI: 10.1021/acscatal.9b02066
ACS Catal. 2019, 9, 8996−9008

involving alkoxides by applying the same scaling factor of 10^{-5} specifically calculated for deprotonation (Table 2).

3.3. Reaction Enthalpies. The enthalpy of reaction on the surface of the zeolite is defined as the sum of the enthalpies of formation of products and reactants, weighted by their stoichiometric coefficients. For example, for a typical oligomerization step between a molecule RH and a protonated intermediate R_1^+:

$$RH + R_1^+ \rightarrow R_2^+ \tag{10}$$

the enthalpy of reaction ΔH_R is expressed as

$$\Delta H_R = \Delta H^f_{phys}(R_2^+) - \Delta H^f_{phys}(R_1^+) - \Delta H^f_{phys}(RH) \tag{11}$$

where ΔH^f_{phys} are the enthalpies of formation of the species in their physisorbed states. The latter can be related to the enthalpies of formation in the gas phase by means of

$$\Delta H^f_{phys}(RH) = \Delta H^f_g(RH) - \Delta H_{phys}(RH) \tag{12}$$

$$\Delta H^f_{phys}(R_1^+) = \Delta H^f_g(R_1^+) - \Delta q(R_1^+) \tag{13}$$

$$\Delta H^f_{phys}(R_2^+) = \Delta H^f_g(R_2^+) - \Delta q(R_2^+) \tag{14}$$

where ΔH^f_g is the enthalpy of formation of the species in the gas phase, ΔH_{phys} is the enthalpy change of a neutral molecular species in going from the gas phase to its physisorbed state within the zeolite pore, and Δq is the stabilization enthalpy of a protonated intermediate.[32] Combining eqs 11−14, the enthalpy of reaction can be finally expressed as

$$\Delta H_R = \Delta H^f_g(R_2^+) - \Delta q(R_2^+) + \Delta q(R_1^+) - \Delta H^f_g(R_1^+) - \Delta H^f_g(RH) + \Delta H_{phys}(RH) \tag{15}$$

or concisely as

$$\Delta H_R = \Delta H_{R,g} - \Delta q(R_2^+) + \Delta q(R_1^+) + \Delta H_{phys}(RH) \tag{16}$$

where $\Delta H_{R,g}$ is the reaction enthalpy in the gas phase.

Generalizing, the reaction enthalpy of every elementary step can be expressed as

$$\Delta H_R = \Delta H_{R,g} + \sum_i \nu_i \cdot \Delta q(R_i^+) + \sum_j \nu_j \cdot \Delta H_{phys}(RH_j) \tag{17}$$

where R_i^+ and RH_j are, respectively, a generic ionic intermediate and a generic molecular species. ν is the stoichiometric coefficient of each species in the elementary step and is defined as positive for products and negative for reactants. The reaction enthalpy in the gas phase was calculated based on Benson's group additivity method[33] using the group additivity values reported in a previous study.[34]

The physisorption enthalpies of the neutral species were estimated depending on the molecule type from linear relationships between physisorption energies and carbon number reported in the literature. From these statistical thermodynamic studies, we deduced that in H-ZSM-5 zeolites, each single-bonded carbon atom provides a contribution of 3.0 kcal mol^{-1},[35] while each double-bonded carbon atom provides a contribution of 5.6 kcal mol^{-1}[36] to the overall physisorption enthalpy of a molecule. However, bimolecular reactions require coadsorption of two molecules at the same Brønsted acid site. After the physisorption of the first molecule, the second molecule adsorbs on the active site-adsorbate complex with a reduced energy (approximately 60% of the physisorption energy of the first molecule at an uncovered Brønsted acid site).[37,38] For this reason, the physisorption energy of this second molecular species involved in the network was calculated as

$$\Delta H_{phys} = c \cdot (3.0 \cdot n_S + 5.6 \cdot n_D) \tag{18}$$

with $c = 0.6$ and where n_S and n_D represent, respectively, the number of single-bonded and double-bonded carbon atoms.

For calculation convenience, we introduced a quantity defined as the stabilization enthalpy of a protonated species relative to the deprotonation enthalpy of the zeolite ($\Delta q(H^+)$ = 295 kcal mol^{-1}[39]), defined as

$$\Delta\Delta q(R^+) = \Delta q(H^+) - \Delta q(R^+) \tag{19}$$

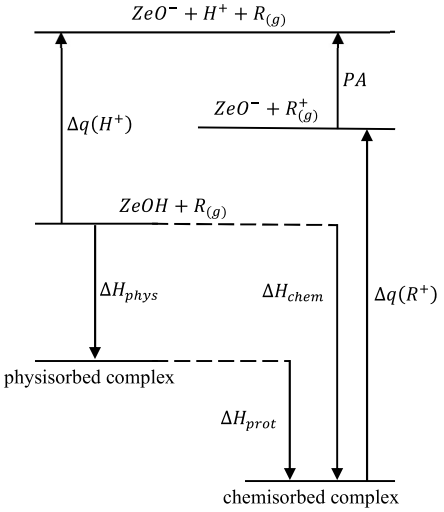

Figure 1. Energy levels used for the estimation of the stabilization energy of the ionic intermediates. Adapted from ref 29. Copyright 2012 American Chemical Society. R in the diagram denotes an olefin.

According to the enthalpy diagram depicted in Figure 1, the stabilization enthalpy of the ionic intermediate R^+ can be expressed as

$$\Delta q(R^+) = -(\Delta H_{chem} - \Delta q(H^+) + PA) \tag{20}$$

where ΔH_{chem} is the chemisorption enthalpy of a gas-phase olefin and PA is its proton affinity. As reported in ref 36, physisorption and chemisorption enthalpies can be considered equal to the corresponding electronic energies in the temperature range 300−800 K. The relative stabilization enthalpy results in the expression in eq 21 accordingly:

$$\Delta\Delta q(R^+) = \Delta H_{chem} + PA \tag{21}$$

The chemisorption enthalpies and the proton affinities of the olefins from C_2 to C_9, together with the calculated relative stabilization enthalpies for the corresponding alkoxides or carbenium ions on H-ZSM-5, are listed in Table 3.

The chemisorption enthalpy of 1-nonene was estimated by extending the linear trend reported for olefins from C_2 to C_9 in ref 36. The increasing trend of the proton affinity with the size of the olefin is rationalized by the electron-donating effect of

DOI: 10.1021/acscatal.9b02066
ACS Catal. 2019, 9, 8996−9008

Table 3. Chemisorption Enthalpies and Proton Affinities of C_2 to C_9 Olefins and Relative Stabilization Enthalpies of the Corresponding Alkoxide or Carbenium Ion on H-ZSM-5

species	π-complex → σ-complex	ΔH_{chem} [kcal/mol]	ref	PA [kcal/mol]	ref	$\Delta\Delta q(R^+)$ [kcal/mol]
primary	ethene → ethoxy	− 31.1	36	168.4	40	137.3
secondary	propene → propoxy	− 33.7	36	179.5	41	145.8
	1-butene → 1-butoxy	−35.1	36	184.7	40	149.6
	1-pentene → 1-pentoxy	−37.3	36	188.1	40	150.8
	1-hexene → 1-hexoxy	−37.0	36	192.4	41	155.4
	1-heptene → 1-heptoxy	−37.8	36			
	1-octene → 1-octoxy	−39.9	36	191.0	40	151.1
	1-nonene → 1-nonoxy	−40.6	estimated	191.0	estimated	150.4
tertiary	isobutene → *t*-butyl	− 17.2	29	195.3	40	178.1

the alkyl chain to stabilize the positive charge of the donated proton. However, this electron-donating effect tends to become attenuated once the alkyl chain of the olefin becomes sufficiently long, as demonstrated by the PA values for olefins between C_3 and C_8 in Table 3. For this reason, the proton affinity of 1-nonene was set equal to that of 1-octene.

The relative stabilization enthalpy of an ionic intermediate depends on the energy level of the protonated species in the gas phase. Thus, it was expressed as a function of the nature of the ionic intermediate and its carbon number using a polynomial expression:

$$\Delta\Delta q(R^+) = \Delta H^{type} + a \cdot n_C + b \cdot {n_C}^2 \quad (22)$$

where ΔH^{type} represents the large contribution of the ionic species type (primary, secondary, or tertiary) to the relative stabilization enthalpy, and n_C is the carbon number of the ionic intermediate. The much smaller contribution $a \cdot n_C + b \cdot {n_C}^2$ to the species' stability accounts for the stabilization effect of the alkyl chain on the distribution of the positive charge.[32] The parameters a, b, and ΔH^{sec} were estimated by fitting the data presented in Table 3 for secondary species with eq 22. The resulting equation was scaled to match the relative stabilization energies of primary and tertiary species, by estimating ΔH^{prim} and ΔH^{tert}. The result of the described fitting procedure is shown in Figure 2 with the parameters listed in Table 4.

It is worth noting that the polynomial expression (eq 22) was specifically referred to the range of carbon number $3 \le n_C \le 9$. The trend of the relative stabilization enthalpy of heavier

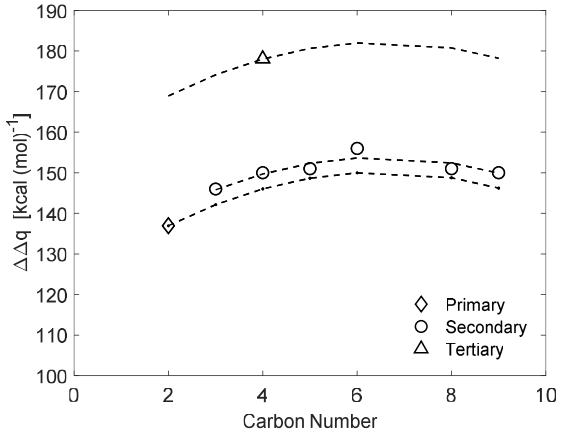

Figure 2. Relative stabilization enthalpies for primary, secondary, and tertiary ionic intermediates as a function of the carbon number in the range $3 \le n_C \le 9$. The dashed lines are regression lines to fit the relative stabilization enthalpies listed in Table 3 using eq 22.

Table 4. Parameters Estimated by Fitting the Relative Stabilization Enthalpies Listed in Table 3 with Equation 22

parameter	value	[−]
a	8.4	
b	− 0.6	
ΔH^{prim}	122.7	kcal/mol
ΔH^{sec}	126.4	kcal/mol
ΔH^{tert}	154.7	kcal/mol

oligomers would be linear with a negative slope dictated by the chemisorption enthalpy change. For this reason, in the event that oligomers with higher carbon number should be included in the model, the following expression is recommended to fit the data:

$$\Delta\Delta q(R^+) = \begin{cases} \Delta H_1^{type} + a_1 \cdot n_C + b_1 \cdot {n_C}^2 & \text{if } 3 \le n_C \le 9 \\ \Delta H_2^{type} + a_2 \cdot n_C & \text{if } n_C > 9 \end{cases} \quad (23)$$

3.2. Activation Energies. According to the Evans–Polanyi relationship, the activation energies were expressed as linear functions of the enthalpy changes associated with the chemical transformations:

$$E_a = E_0 + \alpha\Delta H_R \quad \text{for} \quad \Delta H_R \le 0$$
$$E_a = E_0 + (1 - \alpha)\Delta H_R \quad \text{for} \quad \Delta H_R > 0 \quad (24)$$

where E_0 is the intrinsic energy barrier and ΔH_R is the enthalpy of reaction. α is the transfer coefficient ($0 \le \alpha \le 1$) that characterizes the position of the transition state along the reaction coordinate, such that more exothermic reactions have earlier transition states (α closer to 0) and more endothermic reactions have later transition states (α closer to 1).

For endothermic reactions, the value of E_a was automatically set equal to the enthalpy of reaction, in the event that eq 24 predicted a value lower than the enthalpy of reaction itself. For exothermic reactions, the value of E_a was set equal to zero, in cases where eq 24 predicted a negative value for the activation energy. For thermodynamic consistency, the same value of the energy barrier E_0 was selected for the forward and reverse reaction families (e.g., protonation/deprotonation or oligomerization/β-scission) such that

$$E_{a,forward} - E_{a,reverse} = \Delta H_R \quad (25)$$

The values of the transfer coefficient α were fixed according to the typical reaction enthalpies of the elementary steps included in each reaction family. Values of 0.1 and 0.3 were selected, respectively, for oligomerization and protonation according to

DOI: 10.1021/acscatal.9b02066
ACS Catal. 2019, 9, 8996−9008

the general expectation for highly and moderately exothermic elementary steps.[32] A value of 0.5, which is consistent with a symmetric transition state that has both reactant and product character, was assigned to the isomerization steps.[42]

The intrinsic energy barrier for protonation/deprotonation was distinguished depending on whether the protonated species was an alkoxide (primary or secondary ionic intermediate) or a carbenium ion (tertiary ionic intermediate), to match the experimental observation reported in the literature for isobutene protonation,[29] such that

$$\frac{E_{0,\text{carbenium}}}{E_{0,\text{alkoxide}}} = 0.3 \tag{26}$$

where $E_{0,\text{ carbenium}}$ and $E_{0,\text{ alkoxide}}$ are, respectively, the energy barriers for deprotonation of a carbenium ion or an alkoxide (or of the corresponding protonation). For oligomerization and β-scission, an energy barrier of 19 kcal mol^{-1} was selected by analogy with ref 43. The values of E_0 for the remaining reaction families were estimated during the estimation procedure described in section 5.2.

With the introduction of the Evans–Polanyi relationship, each reaction family can be described by a set of three parameters: a frequency factor A, an intrinsic barrier E_0, and a transfer coefficient α. Estimation of these three parameters required only the calculation of the reaction enthalpy of each elementary step to identify the corresponding reaction rate constants.

4. EXPERIMENTAL METHODS

4.1. Characterization and Pretreatment of MFI Zeolites. The MFI zeolite sample (CBV2314, Si/Al = 13) was obtained from Zeolyst International in NH_4 form. The number of Brønsted acid sites was calculated to be 9.9×10^{-4} mol H^+/g (0.85 H^+/Al) as quantified by NH_3 temperature programed desorption (TPD) of the NH_4-form MFI sample after aqueous phase ion-exchange with NH_4 cations at ambient temperature. Silica (Sigma-Aldrich, high-purity grade, 180–250 μm) was physically mixed with the NH_4-form catalyst (pelleted and sieved to retain 180–250 μm diameter particles) at zeolite–SiO_2 weight ratios of 0.05–0.17, loaded into a stainless-steel reactor (9.5 mm i.d.), and secured by quartz wool plugs and stainless-steel rods on both sides. A concentric thermowell (stainless-steel, 1/8 in. diameter) with a K-type thermocouple extended through the axial center of the reactor. Samples were pretreated in flowing air (1.7×10^{-5} mol/s, zero air, THC < 1 ppm, Indiana Oxygen) and argon (5.1×10^{-5} mol/s, 99.999%, Indiana Oxygen) prior to C_3H_6 oligomerization catalysis to remove physisorbed water and convert the catalyst to its H-form. The reactor temperature was controlled by a furnace (Applied Test Systems series 3210) with a Eurotherm temperature controller (Eurotherm 2408). During pretreatment, the furnace temperature was ramped at 1.5 K/min to 823 K and held for 5 h before cooling to reaction temperature (483–523 K).

4.2. Measurement and Analysis of Oligomerization Rates and Selectivities. Reactant flows were composed of 75% propylene (99.9%, Matheson), 20% argon (99.999%, Indiana Oxygen), and 5% methane (99.97%, Matheson) used as an internal standard. Reactor effluent was flowed through lines heated to 390 K using resistive heating tape (Omegalux) and insulating wrap to a gas chromatograph (Agilent 7890A) equipped with a flame ionization detector (GS GasPro column, 0.320 mm i.d. × 60 m × 0 μm, Agilent) for reactant and product quantification. Reactant space velocity was varied from 1.2 to 9.0 mol C_3 (H^+ s)$^{-1}$ by changing both propylene flow rate (4.8×10^{-5})–(1.1×10^{-4} mol/s) and catalyst mass (10–90 mg) at a fixed propylene partial pressure (165 kPa of propylene, 220 kPa total pressure). Fresh catalyst was loaded for each experiment.

The deactivation profile of molar flow rates of products by carbon number were fit with an exponential decay function[44] and extrapolated to zero time-on-stream for calculation of initial selectivities on a per carbon basis. Conversions were also fit with an exponential decay function and extrapolated to zero time-on-stream. Thus, all reported results reflect initial product formation rates on catalysts prior to deactivation, enabling normalization by *ex-situ* H^+ site counts.

For benchmarking purposes, measured turnover rates on the H-ZSM-5 sample studied here (Si/Al = 13, Zeolyst) were compared to previously reported dimerization turnover rates by Sarazen and co-workers[20] on MFI zeolites at 503 K. All products were assumed to originate from a C_3 dimerization step (i.e., C_6 formation, or products formed from a subsequent reaction of C_6). Dimerization turnover rates (mol C_6 (H^+ s)$^{-1}$) were corrected for deactivation using an exponential decay model (Figure S2) in order to estimate initial turnover rates that can be normalized rigorously by *ex-situ* H^+ site counts.[44] Initial dimerization rates (503 K) were independent of space velocity (Figure S3) and first-order in propene partial pressure (Figure S4), in agreement with previous reports.[20] The apparent first-order dimerization rate constant measured in this work (1.2×10^{-3} m^3 C_6 (H^+ s)$^{-1}$) is comparable to previously reported values (4.8×10^{-4} m^3 C_6 (H^+ s)$^{-1}$).[20] In addition, the selectivity toward secondary products (of β-scission) increases with increasing propylene conversion, consistent with prior work.[13] The consistency of these results with literature reports, and with the current mechanistic understanding of propylene oligomerization at these temperatures and moderate pressures (0–400 kPa propene), indicate that the H-ZSM-5 sample studied here behaves as a representative MFI zeolite. Thus, we used this sample to measure experimental rate and selectivity data at varying temperatures (483–523 K) and propylene conversions (0–4%) to generate data to compare with and aid in the development of the microkinetic model in this study.

Previous work has reported data to indicate that the rates of the initial propylene dimerization step in the oligomerization network are kinetically limited, but that the influence of intrazeolite diffusion on selectivity toward secondary products can be significant.[20] A study from Sarazen et al.[13] showed that the selectivity toward secondary oligomerization products (C_9), as well as the selectivity toward β-scission products, increase as a function of increasing diffusion parameter (a component of the Thiele modulus) but is independent of deprotonation energy (the intrinsic strength of a Brønsted acid site), suggesting that increasing intracrystalline residence times of primary products influence the observed rates of secondary product formation. Therefore, the product selectivity of olefin oligomerization networks may also depend on the zeolite topology and crystallite size because of the influence of intracrystalline mass transfer restrictions that become more pronounced for higher molecular weight products. In this study, we chose not to incorporate transport and diffusion phenomena into the model predictions because the experimental conditions tested led to product distributions (Figure

DOI: 10.1021/acscatal.9b02066
ACS Catal. 2019, 9, 8996–9008

S1, Table S1) containing a majority of dimer products (>65%) and only a minority of secondary oligomerization (~20%) and β-scission products (<5%).

5. RESULTS AND DISCUSSION

5.1. Reaction Network. Figure 3 summarizes the distribution of the 269 gas-phase molecular species and the 371 ionic intermediates included in the reaction network, as a function of carbon number. The same number of molecular species was used to represent the adsorbed-phase molecules. The distribution of the number of generated species shows a typical exponential trend as a function of the carbon number.

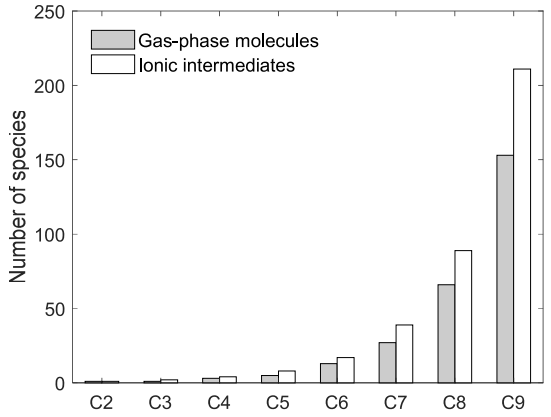

Figure 3. Number of molecular species and ionic intermediates included in the reaction network.

Table 5. Number of Elementary Reactions Included in the Reaction Network

elementary step	no.
protonation	531
deprotonation	531
oligomerization	406
β-scission	406
hydride shift	524
methyl shift	218
α-PCP-branching	504
β-PCP-branching	585
physisorption	269
desorption	269
total	4243

Table 6. Estimated Arrhenius Frequency Factors and Evans–Polanyi Intrinsic Energy Barriers with 95% Confidence Intervals[a]

reaction family	A	[−]	E_0 [kcal mol^{-1}]
protonation	$(8.6 \pm 1.4) \times 10^4$	Pa^{-1} s^{-1}	18.7 ± 1.0
deprotonation	$(1.1 \pm 0.2) \times 10^{14}$	s^{-1}	18.7 ± 1.0
oligomerization	$(9.7 \pm 1.7) \times 10^4$	Pa^{-1} s^{-1}	19.0 ± 0.6
β-scission	$(1.0 \pm 0.1) \times 10^{13}$	s^{-1}	19.0 ± 0.6
hydride shift	$(1.1 \pm 0.2) \times 10^{13}$	s^{-1}	19.8 ± 4.0
methyl shift	$(8.1 \pm 1.1) \times 10^{13}$	s^{-1}	9.0 ± 1.9
α-PCP-branching	$(5.8 \pm 0.5) \times 10^{13}$	s^{-1}	12.5 ± 1.0
β-PCP-branching	$(3.7 \pm 0.7) \times 10^{13}$	s^{-1}	11.3 ± 2.2
physisorption	$(9.9 \pm 1.3) \times 10^0$	Pa^{-1} s^{-1}	
desorption	$(5.6 \pm 0.2) \times 10^7$	s^{-1}	

[a]The frequency factors for deprotonation, oligomerization, β-scission, and isomerization are referred to elementary steps involving alkoxides as reactants. The intrinsic energy barrier for protonation (deprotonation) is referred to as elementary steps involving alkoxides as products (reactants).

A detailed list of the elementary reactions included in the mechanism is presented in Table 5. β-PCP-branching represents the only irreversible steps.

As an interesting point of comparison, a similar network was generated by Shahrouzi et al. for the oligomerization of C_4 olefins on acidic zeolites including 6897 species with a maximum carbon number of 12 and over 35000 elementary reactions.[45] That study only includes ionic intermediates and gas phase molecules, without specifically taking into account the physisorbed species and the physisorption/desorption steps. The application of a $c_{12} - r_0$ termination criterion to the network generation algorithm that is presented in this study would result in the generation of 9015 species and 58542 elementary steps (without including physisorbed species and physisorption/desorption elementary steps). The larger size of this network is related to the presence of primary ionic intermediates which are neglected in the reaction network developed by Shahrouzi et al.[45]

5.2. Parameter Estimation. The reaction rate RR of a generic species i included in the reaction network was expressed in the form:

$$\mathrm{RR}_i = \sum_j \pm A_j \cdot \exp\left(-\frac{E_{a,j}}{RT}\right) \prod_h C_h \tag{27}$$

and incorporated into the design equation of a plug flow reactor. The symbol C_h represents the partial pressure of the hth molecular species or the fractional coverage of the hth ionic intermediate.

The resulting system of 909 ordinary differential equations, describing the change in concentration of each species included in the model, and 1 algebraic equation, describing the mass balance for the surface coverage, was integrated using the DDASAC solver.[46] Parameter estimation was performed using a gradient-based local method (GREG),[47] by minimizing an objective function φ obtained as the sum of the squares of the errors between experimental (σ^{exp}) and calculated (σ^{cal}) conversions and selectivities and expressed as

$$\varphi = \sum_{j=1}^{m} \sum_{i=1}^{n} [w_{i,j}(\sigma_{i,j}^{\mathrm{exp}} - \sigma_{i,j}^{\mathrm{cal}})]^2 \tag{28}$$

with the weighting factors $w_{i,j}$ defined as

$$w_{i,j} = \frac{1}{\sqrt{0.1\sigma_{i,j}^{\mathrm{exp}}}} \tag{29}$$

where n is the number of experimental points, consisting of the product selectivities toward the lumped species C_k ($4 \le k \le 9$) and propylene conversion ($n = 7$). m is the number of experimental runs included in the estimation procedure, conducted at different temperatures, propylene flow rates, and catalyst masses ($m = 6$). The errors between simulated and experimental selectivities were calculated in terms of lumped products (from C_4 to C_9). However, it is worth noting that the model allows the calculation of all the individual product distributions. The conversion of propylene X was expressed as

DOI: 10.1021/acscatal.9b02066
ACS Catal. 2019, 9, 8996−9008

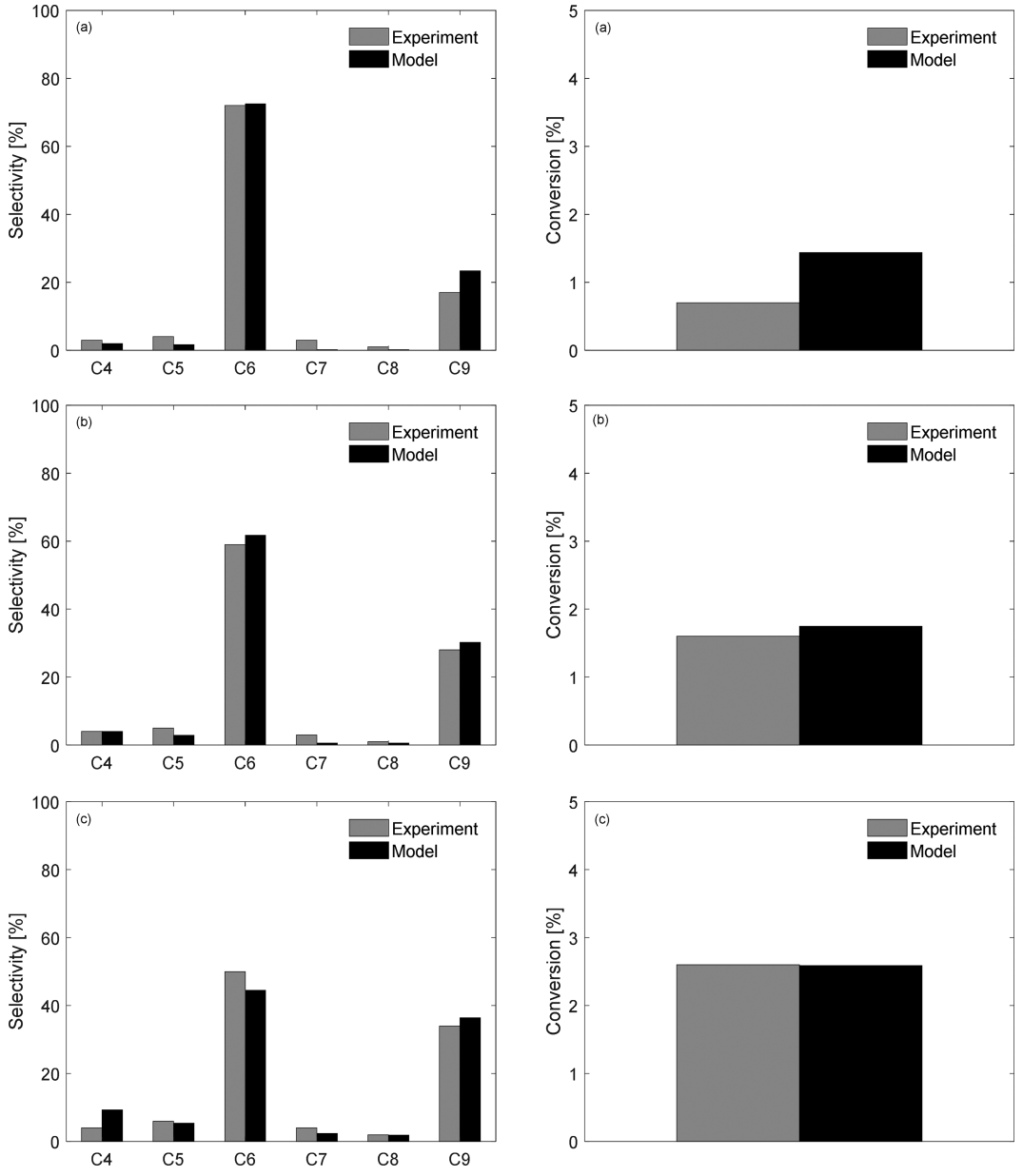

Figure 4. Experimental (gray) and calculated (black) selectivities (left) and conversion (right). Operating conditions: temperature = 503 K; propylene pressure = 165 kPa; propylene flow rate = 1.04×10^{-4} mol s^{-1} (a), 1.07×10^{-4} mol s^{-1} (b), 1.06×10^{-4} mol s^{-1} (c); catalyst mass = 0.017 g (a), 0.027 g (b), 0.051 g (c); calculated space velocities = 6.2 mol_{C3} $(mol_{H+}\ s)^{-1}$ (a), 4.0 mol_{C3} $(mol_{H+}\ s)^{-1}$ (b), 2.1 mol_{C3} $(mol_{H+}\ s)^{-1}$ (c).

$$X = \frac{\sum_{k=4}^{9} k \cdot F_{C_k}}{3F_{C_3H_6}} \tag{30}$$

while the selectivity to the lumped species C_k was calculated as

$$S_{C_k} = \frac{k \cdot F_{C_k}}{\sum_{k=4}^{9} k \cdot F_{C_k}} \tag{31}$$

where F_{C_k} is the molar flow rate of the lumped species C_k and $F_{C_3H_6}$ is the molar flow rate of propylene fed to the reactor. During this estimation procedure, the frequency factors and the intrinsic barriers E_0 were tuned to fit the experimental data. A total of $n \cdot m$ = 42 experimental data points at two temperatures (503 and 523 K), varying propylene flow rates, and catalyst loadings (as described in section 4) were used to estimate 19 parameters (10 Arrhenius frequency factors, 8 intrinsic energy barriers, and the ratio of frequency factors for all the elementary steps that involved carbenium ions and alkoxides as reactants). The estimation process converged once the relative change of each parameter was smaller than 10^{-5}.

The values of the kinetic parameters resulting from the estimation procedure are listed in Table 6 with their 95% confidence intervals, where the frequency factors for deprotonation, oligomerization, β-scission, and isomerizations are referred to elementary steps involving alkoxides as reactants. The intrinsic energy barrier for protonation, reported in Table 6, is referred to as elementary steps involving alkoxides as products. In the same way, the energy barrier for deprotonation is referred to elementary steps involving alkoxides as reactants. The corresponding values for carbenium ions can be calculated using eq 26. The estimated intrinsic energy barriers range between 9 and 20 kcal mol^{-1}, in reasonable agreement with those reported in the literature.[32,48]

DOI: 10.1021/acscatal.9b02066
ACS Catal. 2019, 9, 8996−9008

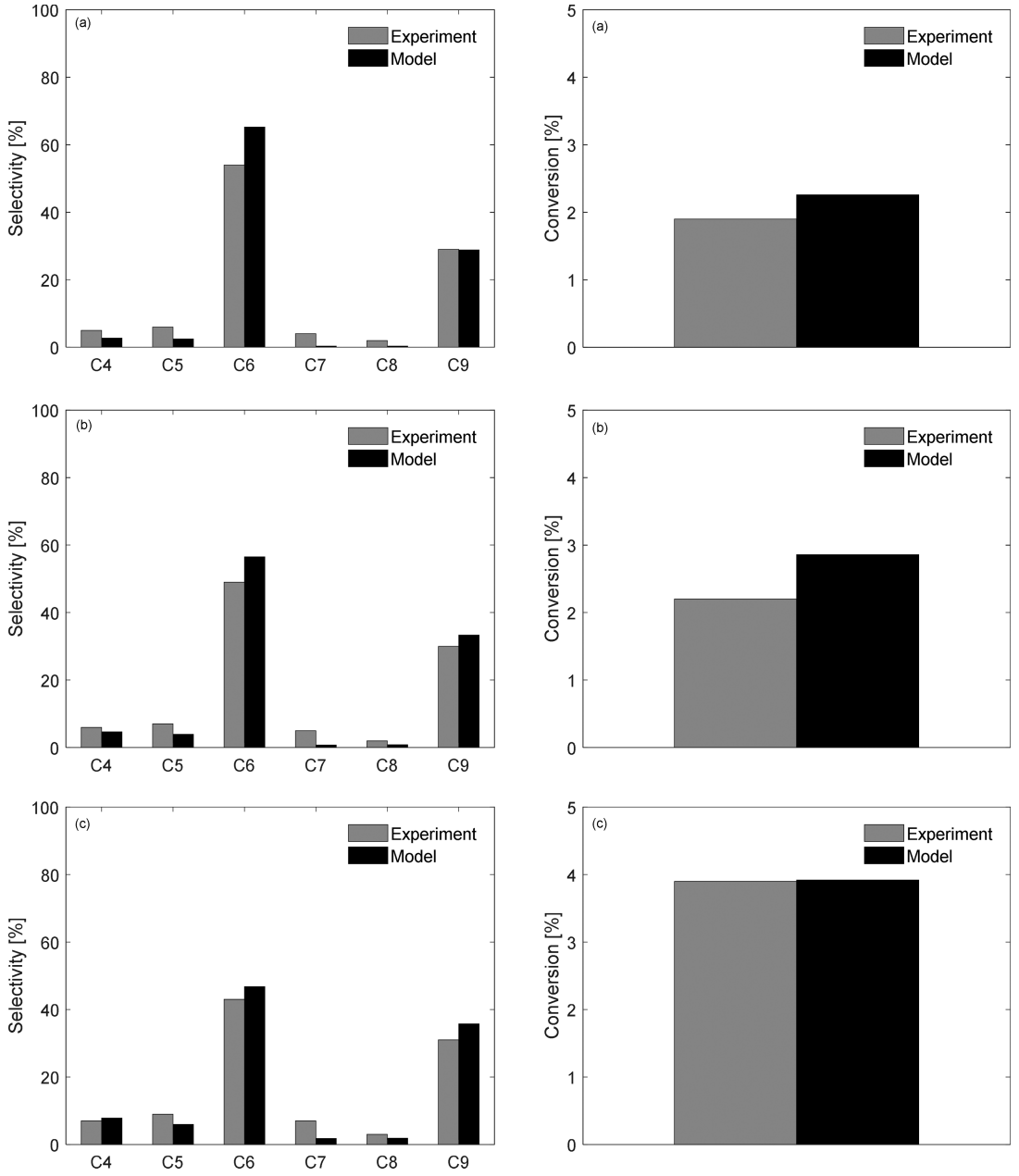

Figure 5. Experimental (gray) and calculated (black) selectivities (left) and conversion (right). Operating conditions: temperature = 523 K; propylene pressure = 165 kPa; propylene flow rate = 1.07×10^{-4} mol s^{-1} (a), 1.04×10^{-4} mol s^{-1} (b), 1.10×10^{-4} mol s^{-1} (c); catalyst mass = 0.012 g (a), 0.017 g (b), 0.027 g (c). Calculated space velocities = 9.0 mol_{C3} $(mol_{H+}\ s)^{-1}$ (a), 6.2 mol_{C3} $(mol_{H+}\ s)^{-1}$ (b), 4.1 mol_{C3} $(mol_{H+}\ s)^{-1}$ (c).

The ratio of frequency factors for all the elementary steps that involved carbenium ions and alkoxides as reactants, respectively, $A_{carbenium}$ and $A_{alkoxide}$, was estimated to be

$$\frac{A_{carbenium}}{A_{alkoxide}} = (1.4 \pm 0.3) \times 10^{-5} \tag{32}$$

The values of the estimated frequency factors fall within an order of magnitude of those calculated using transition state theory, with the only exception being that for β-scission (difference of 1 order of magnitude). This slight disagreement was ascribed to the termination criterion used during the automated generation of the reaction network. The termination criterion described in section 2 generates C_9 ionic intermediates that are not allowed to react with propylene. The occurrence of β-scission reactions transforms these species into smaller ionic intermediates that react with propylene molecules, resulting in higher conversion. As a consequence of the truncated reaction network, a higher value of the frequency factor for β-scission resulted in overestimated conversions that were not in agreement with the observed experimental data. We note that the values obtained for E_0 of hydride and methyl shift reactions might be expected to be closer, given the general similarity of these reaction families. However, forcing them to be closer resulted in a larger discrepancy of the frequency factors compared to estimates using transition state theory, so their initial estimates were retained. A detailed study using theory to specifically examine these two reaction families would be valuable to explore these E_0 values further.

DOI: 10.1021/acscatal.9b02066
ACS Catal. 2019, 9, 8996−9008

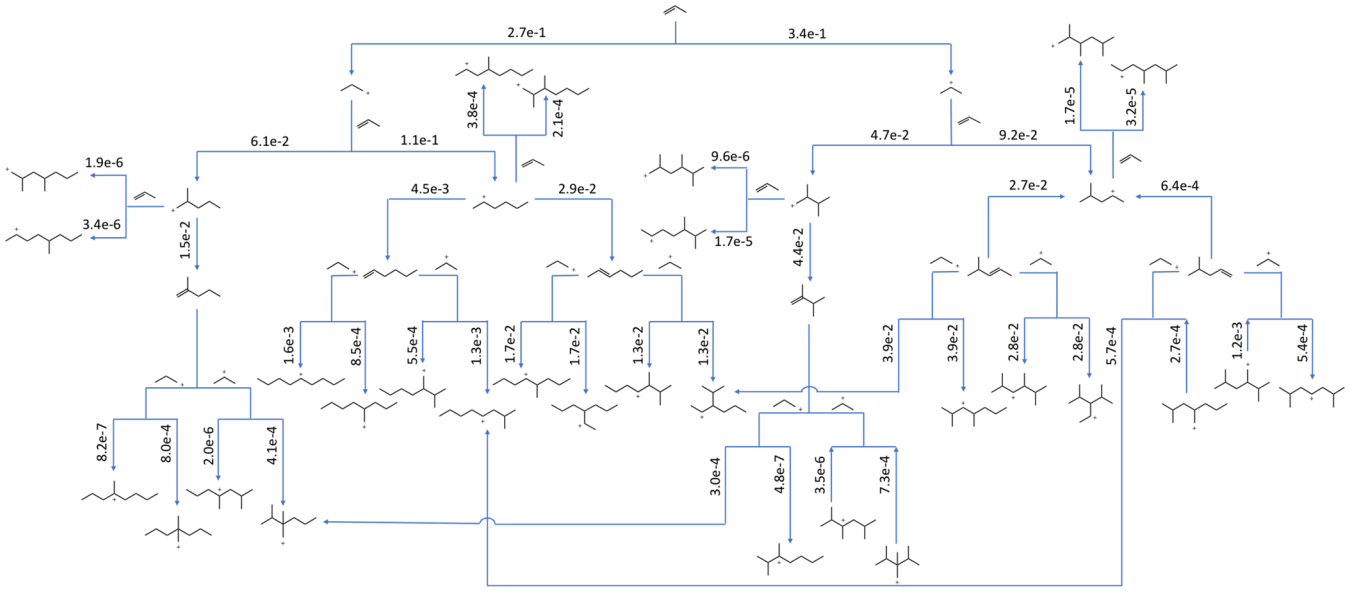

Figure 6. Net rate in s^{-1} of a section of the propylene oligomerization network. All isomerizations and deprotonation of C_9 ionic intermediates are not shown for simplicity. The arrows point to species with a positive rate of formation. Operating conditions: temperature = 503 K; propylene pressure = 165 kPa; propylene flow rate = 1.04×10^{-4} mol s^{-1}; catalyst mass = 0.017 g; calculated space velocity = 6.2 mol_{C3} $(mol_{H+}\ s)^{-1}$.

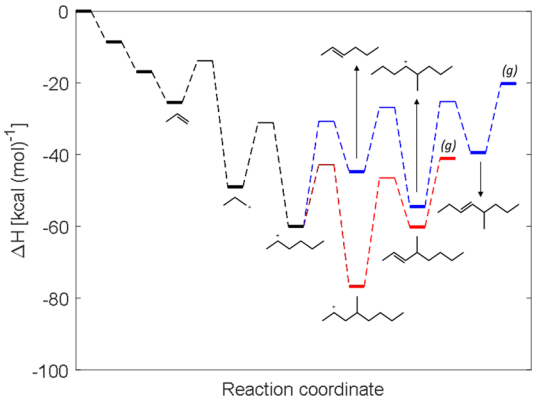

Figure 7. Schematic reaction coordinate diagram for an exemplar propylene oligomerization pathway. In red: addition of physisorbed propylene to 2-hexoxide and formation of 4-methyl-2-octene. In blue: addition of 1-propoxide to physisorbed 2-hexene and formation of 5-methyl-3-octene. Thin horizontal lines indicate transition states.

5.3. Model Execution. Comparison of the experimental selectivities and conversion values and the best fit of the microkinetic model are presented in Figure 4 (503 K) and Figure 5 (523 K). Increasing propylene conversion results in a lower selectivity to C_6 species and in a higher selectivity to secondary oligomerization products (C_9) and to cracking species (C_4, C_5, C_7, C_8). C_6 olefins represent the most abundant products with a significant prevalence of isomers containing internal double bonds (~70%) over those containing terminal double bonds.

The proposed model is able to capture the reactant conversion and the selectivity of the process to major and minor products with very good accuracy over the range of operating conditions that was investigated. It is worth noting that the model describes significant variations in the product selectivity that result from minor changes in propylene conversion over a narrow range (0–4%).

Figure 6 shows a small section of the oligomerization network that involves primary and secondary oligomerization steps of propylene to C_6 and C_9 species with net rates expressed in s^{-1}. Isomerization steps and deprotonation of C_9 molecular species are not shown for simplicity. The arrows point to species with a positive rate of formation. The quasi-equilibrated formation of primary and secondary propoxides that differ in the carbon atom bound to the zeolite framework occurs after interaction of propylene with the acid sites. The model shows that at low propylene conversion (<4%), these species coexist at comparable coverages near saturation (>90%), in agreement with propylene dimerization rates that result in an apparent first-order dependence on propylene pressure (Figure S4). This is confirmed by infrared spectroscopy data reported by Sarazen et al. showing that the protonation of propylene at moderate pressure (10–500 kPa) on MFI leads to equilibrated mixtures of primary and secondary propoxides with similar energies of formation.[20] The first oligomerization step results in the formation of four alkoxides after addition of a molecule of propylene to a propoxide: 2-methyl-1-pentoxide, 2-hexoxide, 2,3-dimethyl-1-butoxide, and 4-methyl-2-pentoxide, with a preferential formation of secondary alkoxides. The subsequent secondary oligomerization of a C_6 ionic intermediate to a C_9, in the range of investigated conditions resulting in low conversion, is less favorable than its corresponding deprotonation and results in

$$k_{dp} \gg k_{olig} \cdot p_{C_3H_6} \tag{33}$$

where k_{dp} and k_{olig} are, respectively, the rate constants of a C_6 alkoxide deprotonation and oligomerization, and $p_{C_3H_6}$ is the propylene partial pressure in the pores of the zeolite.

This suggests that, at low conversion, the formation of C_9 species is driven by the addition of propoxides to physisorbed C_6 molecules. Figure 7 shows an exemplar reaction coordinate diagram for the oligomerization pathway of propylene to form 4-methyl-2-octene (in red) through addition of propylene to 2-hexoxide and to form 5-methyl-3-octene (in blue) through addition of 1-propoxide to 2-hexene. The symbol (g) indicates molecular species in the gas phase. The blue pathway is thermodynamically disfavored because it requires the endo-

DOI: 10.1021/acscatal.9b02066
ACS Catal. 2019, 9, 8996–9008

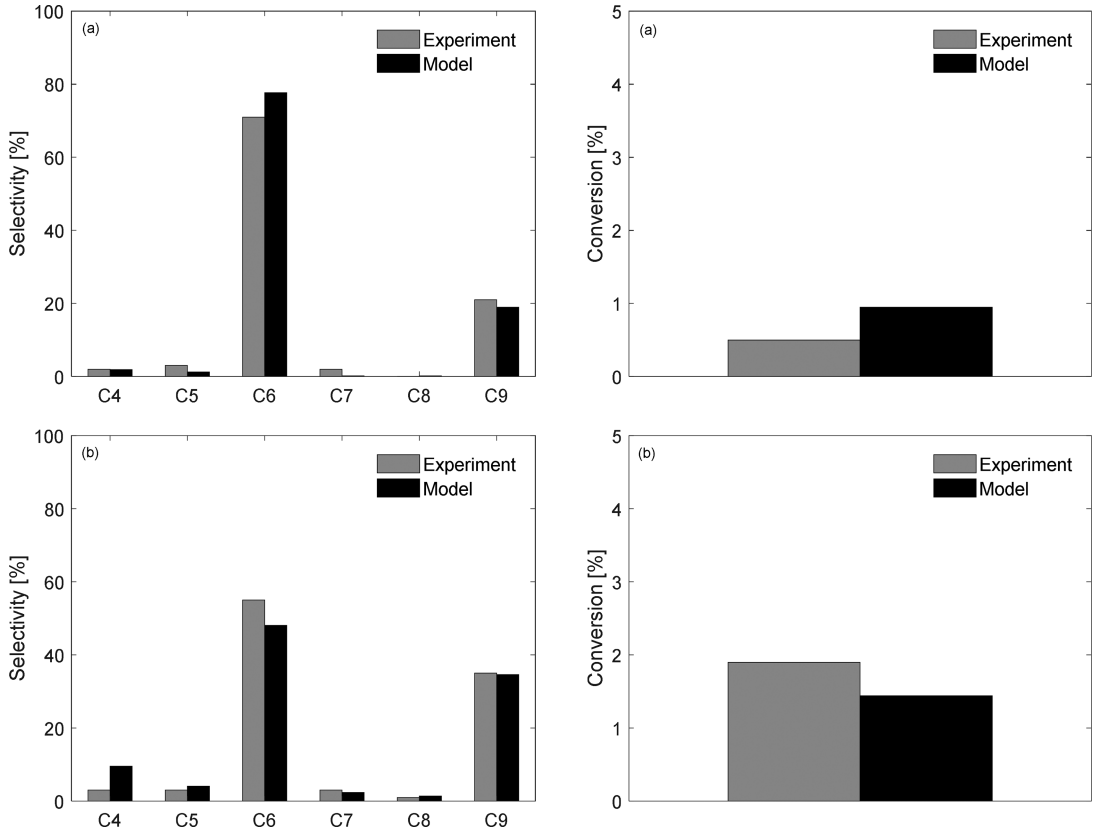

Figure 8. Model prediction: Comparison between experimental (gray) and calculated (black) selectivities (left) and conversion (right). Operating conditions: temperature = 483 K; propylene pressure = 165 kPa; propylene flow rate = 6.77×10^{-5} mol s^{-1} (a), 1.03×10^{-4} mol s^{-1} (b); catalyst mass = 0.019 g (a), 0.087 g (b). Calculated space velocities = 3.6 mol_{C3} $(mol_{H+}\ s)^{-1}$ (a), 1.2 mol_{C3} $(mol_{H+}\ s)^{-1}$ (b).

thermic deprotonation of 2-hexoxide. However, it is kinetically favored as demonstrated in Figure 6, wherein 5-methyl-4-octoxide is formed with a rate of 1.7×10^{-2} s^{-1}. At low conversion, the primary and secondary propoxides are present at saturation coverage on the surface of the zeolite. For this reason, in the range of investigated conditions, a physisorbed molecule of 2-hexene preferentially undergoes oligomerization and not protonation, resulting in

$$k^{*}_{olig} \cdot \vartheta_{propox} > k_{pt} \cdot \vartheta_{0} \quad (34)$$

where k^{*}_{olig} and k_{pt} are the rate constants of oligomerization and protonation of a C_6 molecular species, and ϑ_{propox} and ϑ_0 are the fractional surface coverages of propoxides and vacant sites, respectively.

5.4. Model Validation. A validation of the microkinetic model was conducted by extending the simulation to additional experiments that were not included among those previously used during parameter estimation, at an additional operating temperature (483 K) outside of the range used during estimation. During this phase, the estimated values for the parameters were used to predict the experimental values without any additional adjustment. Comparison between experimental data and model prediction are shown in Figure 8.

6. CONCLUSIONS

In this work, a microkinetic model was developed to describe the oligomerization of propylene on a representative H-ZSM-5 zeolite over a conversion range lower than 4%. An automated network generation mechanism was applied to build a reaction mechanism consisting of 4243 elementary steps and 909 species including ionic intermediates and gas-phase and physisorbed molecular species within the C_2−C_9 carbon range. The collected experimental results helped elucidate the prevalent elementary steps that were grouped into eight reaction families. Each reaction family was described by a set of three parameters: a frequency factor A, an intrinsic barrier E_0, and a transfer coefficient α. With these parameters specified, only the calculation of the reaction enthalpy of each elementary step was required to identify the corresponding reaction rate constants. Both experimental and modeling results indicated that increasing propylene conversion results in a lower selectivity toward dimer species (C_6) and a higher selectivity toward secondary oligomerization products (C_9) and to cracking species (C_4, C_5, C_7, C_8).

The model revealed the presence of bound alkoxides at near saturation coverages during the oligomerization process at low conversion. Analysis of resultant net rates showed that, at low conversion, the addition of propoxides to physisorbed C_6 olefins drives the oligomerization process toward C_9 species.

Very good agreement with experimental conversions and selectivities over a wide range of operating conditions demonstrated that the model is robust and suggests that it is extendable to additional olefins and acidic zeolites. The developed microkinetic model is a powerful tool to simulate the behavior of the Brønsted acid-based oligomerization process, predict the product distribution, and facilitate catalyst design efforts to achieve a more tailored product specification.

DOI: 10.1021/acscatal.9b02066
ACS Catal. 2019, 9, 8996−9008

■ ASSOCIATED CONTENT

Supporting Information

The Supporting Information is available free of charge on the ACS Publications website at DOI: 10.1021/acscatal.9b02066.

Product distribution of propylene reactions on H-ZSM-5, experimental analysis of rate and selectivity data, model reduction, and simulated selectivity and conversion profiles along the PFR (PDF)

■ AUTHOR INFORMATION

Corresponding Author

*E-mail: broadbelt@northwestern.edu.

ORCID

Sergio Vernuccio: 0000-0003-1254-0293
Rajamani Gounder: 0000-0003-1347-534X
Linda J. Broadbelt: 0000-0003-4253-592X

Notes

The authors declare no competing financial interest.

■ ACKNOWLEDGMENTS

This paper is based upon work supported primarily by the National Science Foundation under Cooperative Agreement No. EEC-1647722. Any opinions, findings, and conclusions or recommendations expressed in this material are those of the author(s) and do not necessarily reflect the views of the National Science Foundation.

■ REFERENCES

(1) Scurrell, M. S. Prospects for the Direct Conversion of Light Alkanes to Petrochemical Feedstocks and Liquid Fuels - a Review. *Appl. Catal.* **1987**, *32*, 1−22.

(2) Brandt, A. R. Converting Oil Shale to Liquid Fuels: Energy Inputs and Greenhouse Gas Emissions of the Shell in Situ Conversion Process. *Environ. Sci. Technol.* **2008**, *42*, 7489−7495.

(3) Ridha, T.; Li, Y.; Gençer, E.; Siirola, J. J.; Miller, J. T.; Ribeiro, F. H.; Agrawal, R. Valorization of Shale Gas Condensate to Liquid Hydrocarbons through Catalytic Dehydrogenation and Oligomerization. *Processes* **2018**, *6*, 139−160.

(4) Labinger, J. A.; Leitch, D. C.; Bercaw, J. E.; Deimund, M. A.; Davis, M. E. Upgrading light hydrocarbons: a tandem catalytic system for alkane/alkene coupling. *Top. Catal.* **2015**, *58*, 494−501.

(5) Guisnet, M., Gilson, J. P., Eds. *Zeolites for Cleaner Technologies*; Imperial College Press: London, U.K., 2002; pp 1−28.

(6) Jacobs, P. A.; Martens, J. A. *Introduction to Zeolite Science and Practice*; van Bekkum, H., Jacobs, P. A., Flanigen, E. M., Jansen, J. C., Eds.; Elsevier: New York, 1991; pp 445−496.

(7) Garwood, W. E.; Caesar, P. D.; Brennan, J. A. *Light olefin processing*. U.S. Patent 4,150,062, April 17, 1979.

(8) Garwood, W. E.; Lee, W. *Process for separating ethylene from light olefin mixtures while producing both gasoline and fuel oil*. U.S. Patent 4,227,992, October 14, 1980.

(9) Tabak, S. A. *Oligomerization of olefins*. U.S. Patent 4,254,295, March 3, 1981.

(10) Tabak, S. A.; Wright, B. S.; Owen, H. *Catalytic conversion of olefins to heavier hydrocarbons*. U.S. Patent 4,504,693, March 12, 1985.

(11) Quann, R. J.; Green, L. A.; Tabak, S. A.; Krambeck, F. J. Chemistry of Olefin Oligomerization over ZSM-5 Catalyst. *Ind. Eng. Chem. Res.* **1988**, *27*, 565−570.

(12) Bellussi, G.; Mizia, F.; Calemma, V.; Pollesel, P.; Millini, R. Oligomerization of olefins from Light Cracking Naphtha over zeolite-based catalyst for the production of high quality diesel fuel. *Microporous Mesoporous Mater.* **2012**, *164*, 127−134.

(13) Sarazen, M. L.; Doskocil, E.; Iglesia, E. Effects of Void Environment and Acid Strength on Alkene Oligomerization Selectivity. *ACS Catal.* **2016**, *6*, 7059−7070.

(14) Mohammed, A. A.; Fateen, S.-E. K.; Ahmed, T. S.; Moustafa, T. M. A kinetic model for ethylene oligomerization using zirconium/aluminum- and nickel/zinc-based catalyst systems in a batch reactor. *Appl. Petrochem. Res.* **2014**, *4*, 287−295.

(15) Paynter, J. D.; Schuette, W. L. Development of a model for kinetics of olefin codimerization. *Ind. Eng. Chem. Process Des. Dev.* **1971**, *10*, 250−257.

(16) Cao, G.; Viola, A.; Baratti, R.; Morbidelli, M.; Sanseverino, L.; Cruccu, M. Lumped Kinetic model for propene-butene mixtures oligomerization on a supported phosphoric acid catalyst. *Appl. Catal.* **1988**, *41*, 301−312.

(17) Vernuccio, S.; Broadbelt, L. J. Discerning complex reaction networks using automated generators. *AIChE J.* **2019**, *65*, e16663.

(18) Broadbelt, L. J.; Stark, S. M.; Klein, M. T. Computer-Generated Pyrolysis Modeling − On-the-Fly Generation of Species, Reactions, and Rates. *Ind. Eng. Chem. Res.* **1994**, *33* (4), 790−799.

(19) Klein, M. T.; Hou, G.; Bertolacini, R. J.; Broadbelt, L. J.; Kumar, A. *Molecular Modeling in Heavy Hydrocarbon Conversions*; CRC Press, Taylor & Francis Group: Boca Raton, FL, 2006.

(20) Sarazen, M. L.; Doskocil, E.; Iglesia, E. Catalysis on solid acids: Mechanism and catalyst descriptors in oligomerization reactions of light alkenes. *J. Catal.* **2016**, *344*, 553−569.

(21) Cnudde, P.; De Wispelaere, K.; Van der Mynsbrugge, J.; Waroquier, M.; Van Speybroeck, V. Effect of temperature and branching on the nature and stability of alkene cracking intermediates in H-ZSM-5. *J. Catal.* **2017**, *345*, 53−69.

(22) Brouwer, D. M.; Hogeveen, H. Electrophilic Substitutions at Alkanes and in Alkylcarbonium Ions. *Prog. Phys. Org. Chem.* **2007**, *9*, 179−240.

(23) von Aretin, T.; Schallmoser, S.; Standl, S.; Tonigold, M.; Lercher, J. A.; Hinrichsen, O. Single-Event Kinetic Model for 1-Pentene Cracking on ZSM-5. *Ind. Eng. Chem. Res.* **2015**, *54* (47), 11792−11803.

(24) von Aretin, T.; Standl, S.; Tonigold, M.; Hinrichsen, O. Optimization of the product spectrum for 1-pentene cracking on ZSM-5 using single-event methodology. Part 2: Recycle reactor. *Chem. Eng. J.* **2017**, *309*, 873−885.

(25) Ying, L.; Zhu, J.; Cheng, Y.; Wang, L.; Li, X. Kinetic modeling of C2−C7 olefins interconversion over ZSM-5 catalyst. *J. Ind. Eng. Chem.* **2016**, *33*, 80−90.

(26) Standl, S.; Tonigold, M.; Hinrichsen, O. Single-Event Kinetic Modeling of Olefin Cracking on ZSM-5: Proof of Feed Independence. *Ind. Eng. Chem. Res.* **2017**, *56*, 13096−13108.

(27) Broadbelt, L. J.; Stark, S. M.; Klein, M. T. Termination of Computer-Generated Reaction Mechanisms: Species Rank-Based Convergence Criterion. *Ind. Eng. Chem. Res.* **1995**, *34* (8), 2566−2573.

(28) Robinson, P. J. Dimensions and standard states in the activated complex theory of reaction rates. *J. Chem. Educ.* **1978**, *55* (8), 509−510.

(29) Nguyen, C. M.; De Moor, B. A.; Reyniers, M.-F.; Marin, G. B. Isobutene protonation in H-FAU, H-MOR, H-ZSM-5, and H-ZSM-22. *J. Phys. Chem. C* **2012**, *116*, 18236−18249.

(30) Buchanan, J. S.; Santiesteban, J. G.; Haag, W. O. Mechanistic considerations in acid-catalyzed cracking of olefins. *J. Catal.* **1996**, *158*, 279−287.

(31) Mazar, M. N.; Al-Hashimi, S.; Cococcioni, M.; Bhan, A. *β*-Scission of olefins on acidic zeolites: a periodic PBE-D study in H-ZSM-5. *J. Phys. Chem. C* **2013**, *117*, 23609−23620.

(32) Martinis, J. M.; Froment, G. F. Alkylation on solid acids. Part 2. Single-event kinetic modeling. *Ind. Eng. Chem. Res.* **2006**, *45*, 954−967.

(33) Benson, S. W. *Thermochemical Kinetics: Methods for the Estimation of Thermochemical Data and Rate Parameters*; John Wiley, Inc.: New York, 1976.

DOI: 10.1021/acscatal.9b02066
ACS Catal. 2019, 9, 8996−9008

(34) Bjorkman, K.; Sung, C.; Mondor, E.; Cheng, J. C.; Jan, D.-Y.; Broadbelt, L. J. Group additivity determination for enthalpies of formation of carbenium ions. *Ind. Eng. Chem. Res.* **2014**, *53*, 19446−19452.
(35) De Moor, B. A.; Reyniers, M. F.; Gobin, O. C.; Lercher, J. A.; Marin, G. B. Adsorption of C2-C8 n-Alkanes in Zeolites. *J. Phys. Chem. C* **2011**, *115*, 1204−1219.
(36) Nguyen, C. M.; De Moor, B. A.; Reyniers, M. F.; Marin, G. B. Physisorption and Chemisorption of Linear Alkenes in Zeolites: A Combined QM-Pot(MP2//B3LYP:GULP)-Statistical Thermodynamics Study. *J. Phys. Chem. C* **2011**, *115*, 23831−23847.
(37) Moses, P. G.; Norskov, J. K. Methanol to Dimethyl Ether over ZSM-22: A Periodic Density Functional Theory Study. *ACS Catal.* **2013**, *3*, 735−745.
(38) Fang, Z.; Wang, Y.; Dixon, D. A. Computational Study of Ethanol Conversion on Al_8O_{12} as a Model for γ-Al_2O_3. *J. Phys. Chem. C* **2015**, *119*, 23413−23421.
(39) Nguyen, C. M.; Reyniers, M.-F.; Marin, G. B. Adsorption thermodynamics of C1-C4 alcohols in H-FAU, H-MOR, H-ZSM-5, and H-ZSM-22. *J. Catal.* **2015**, *322*, 91−103.
(40) De Moor, B. A.; Reyniers, M. F.; Sierka, M.; Sauer, J.; Marin, G. B. Physisorption and chemisorption of hydrocarbons in H-FAU using QM-Pot(MP2//B3LYP) calculations. *J. Phys. Chem. C* **2008**, *112*, 11796−11812.
(41) Hunter, E. P.; Lias, S. G. Evaluated gas phase basicities and proton affinities of molecules: an update. *J. Phys. Chem. Ref. Data* **1998**, *27* (3), 413−656.
(42) Oakley, L. H.; Casadio, F.; Shull, K. R.; Broadbelt, L. J. Theoretical Study of Epoxidation Reactions Relevant to Hydrocarbon Oxidation. *Ind. Eng. Chem. Res.* **2017**, *56*, 7454−7461.
(43) Shen, W. A theoretical study of confinement effect of zeolite on the ethylene dimerization reaction. *Microporous Mesoporous Mater.* **2017**, *247*, 136−144.
(44) Costa, C.; Lopes, J. M.; Lemos, F.; Ramoa Ribeiro, F. Activity−acidity relationship in zeolite Y: Part 1. Transformation of light olefins. *J. Mol. Catal. A: Chem.* **1999**, *144*, 207−220.
(45) Shahrouzi, J. R.; Guillaume, D.; Rouchon, P.; Da Costa, P. Stochastic simulation and single events kinetic modeling: Application to olefin oligomerization. *Ind. Eng. Chem. Res.* **2008**, *47*, 4308−4316.
(46) Stewart, W. E.; Caracotsios, M.; Sorensen, J. P. *Double Precision Differential-Algebraic Sensitive Analysis Code*, Version 1997, Vol. 3; Wisconsin University: Madison, WI, 1997.
(47) Stewart, W. E.; Caracotsios, M.; Sorensen, J. P. *Generalized regression software (GREG)*, Version 1997, Vol. 3; Wisconsin University: Madison, WI, 1997.
(48) Watson, B. A.; Klein, M. T.; Harding, R. H. Mechanistic modeling of n-heptene cracking on HZSM-5. *Ind. Eng. Chem. Res.* **1996**, *35*, 1506−1516.

NOTE ADDED AFTER ASAP PUBLICATION

This paper was published on the Web on September 4, 2019 with missing molecules in Figure 7. Figure 7 was replaced, and corrected version was reposted on September 6, 2019.

DOI: 10.1021/acscatal.9b02066
ACS Catal. 2019, 9, 8996−9008